Porosity of growing sea ice and potential for oil entrainment

Chris Petrich*

Northern Research Institute, Narvik, Norway

Jonas Karlsson

University of Copenhagen, Copenhagen, Denmark

Hajo Eicken

Geophysical Institute and International Arctic Research Center, University of Alaska Fairbanks, Fairbanks, Alaska, USA

*Corresponding author email: christian.petrich@norut.no

Highlights

- Sea ice porosity from multiple years of ice temperature and salinity measurements.
- Depth of potential oil entrainment estimated.
- Entrainment depth increased from <0.02 m in January to >0.1 to 0.2 m in May.
- Interstitial entrainment adds approximately 20% to under-ice pooling capacity.

Abstract

The pore space in the bottom-most layers of growing sea ice is directly connected to the ocean beneath, allowing for fluid exchange while providing a sheltered environment for sea-ice microbial communities. Because of its role as a habitat and its high porosity and permeability, potential entrainment of oil into this pore space is of broader concern. We estimate the ice volume that can potentially be infiltrated by oil and other buoyant pollutants in surface ocean water evaluating several years of sea ice measurements on undeformed landfast first-year sea ice at Barrow, Alaska. This ice is representative of undeformed sea ice in areas targeted for offshore oil development. The calculated ice volume is related to crude oil entrainment volumes with empirical relationships derived from field and laboratory measurements. We synthesize 12 years of sea-ice core salinity data and 6 years of quasi-continuous sea ice temperature profile measurements to derive the seasonal evolution of ice thickness and temperature gradients in sea ice. Porosity profiles are calculated from temperature and salinity profiles. Based on previous observations, an oil penetration depth is defined by a porosity threshold of 0.1 to 0.15. Ice thickness is found to increase from 0.6 m in January to its maximum of 1.5 m in May, and average temperature gradients at the ice–water interface range from -15 °C/m in January to -2 °C/m in May. Depending on ice temperature conditions, derived depths of fluid penetration range from 0.02 to 0.10 m in January to 0.12 to 0.25 m in May for a porosity threshold of 0.10. These penetration depths are approximately halved for a porosity threshold of 0.15. For average temperature conditions, expected entrainment of crude oil is less than 2 L/m^2 in January and may be as high as 5 to 10 L/m^2 in May. Accessible ice volume and entrainment potential are expected to increase during warm spells and with the opening of brine channel networks in late spring. Considering inhomogeneous spread and pooling of oil under ice, entrainment in warm sea ice is expected to add approximately 20% to previous estimates of the under-ice pooling capacity.

Keywords: sea ice, porosity, oil

Introduction

Sea ice is a porous material that exchanges fluid with the underlying ocean during growth (e.g., Eide and Martin, 1975). This creates a small-scale marine environment that is both sheltered and connected to the ocean underneath. Thus, the bottom layers of sea ice are known to serve as a biological habitat (Cota and Smith, 1991; Krembs et al., 2000; Gradinger et al., 2009) but are also susceptible to entrainment and retention of oil spilled under the ice (e.g., Wolfe and Hoult, 1974; NORCOR, 1975; Otsuka et al., 2004; Buist et al., 2008; Karlsson et al., 2011). Most of the fluid exchange is confined to the region near the ice–water interface where the volume fraction and morphology of the pore space are challenging to quantify (e.g., Cox and Weeks, 1975; Weissenberger et al., 1992; Krembs et al., 2000; Notz and Worster, 2008). However, past field and laboratory measurements indicate that volume-averaged bulk oil entrainment is dependent on a porosity threshold that separates ice susceptible to infiltration from that that is not susceptible (e.g. NORCOR, 1975; Karlsson et al., 2011). Based on those observations and 12 years of measurements of physical properties of landfast, first-year sea ice at Barrow, Alaska, the accessible sea ice volume and potential entrainment volume of oil is estimated in this study. The focus of this study is on growing columnar ice with a lamellar ice–ocean interface, i.e. not including granular ice or thin sea ice, or ice with protruding platelets (Jeffries et al., 1995; Petrich and Eicken, 2010). Oil infiltration into this ice type has been investigated in field and laboratory experiments used in the present study (NORCOR, 1975; Karlsson, 2009; Karlsson et al., 2011).

Modes of interaction between oil and sea ice have been reviewed by Fingas and Hollebone (2003). Oil impinging on the underside of sea ice spreads laterally as a film or as discrete droplets. The lateral extent of spread is limited by the bottom topography of sea ice, which gives rise to the concept of pooling capacity (e.g., Wilkinson et al. 2007). Once the oil is stationary, a lip of sea ice will grow over the oil lens, encapsulating and immobilizing oil. Ice above the oil lens entrains oil into the connected brine pore space, such that the oil extends through the skeletal layer (the lowermost layer exhibiting high porosities and no mechanical strength) into the ice above and into brine channels. Dickins (1992) reviewed laboratory and field studies that investigated oil entrainment in sea ice. Summaries of more recent work were provided, among others, by Buist et al. (2008) and Dickins (2011). For the purpose of this study, the most relevant and detailed data on oil entrainment in ice are those of NORCOR (1975) and Martin (1979) for field work, and Otsuka et al. (2004) and Karlsson et al. (2011) for laboratory studies.

One of the first studies investigating the fate of oil released under sea ice from winter through spring was the NORCOR experiment in landfast first-year sea ice in the Canadian Arctic (NORCOR, 1975;

Martin, 1979). It demonstrated that most of the oil spilled in fall and winter was entrained as lenses pooling under and then encapsulated in the ice. In spring, as the ice started to warm, oil began to migrate upward as brine channels increased in size. Eventually, oil reached the surface through discrete channels in May. As the ice continued to deteriorate, the oil progressively saturated the interstices within and between ice crystals. Oil continued to flow upward through the ice until surface ablation had fully exposed the level of initial oil-lens entrainment. The average concentration of oil in oil-saturated sea ice was 4.5%, with a maximum of 7% in a 4 cm section.

Recently, Karlsson et al. (2011) reported on results of laboratory experiments on oil entrainment in sea ice. They grew ice to approximately 0.15 m thickness, injected oil under the ice, allowed the oil lens to become encapsulated, raised the ambient temperature in some experiments, and then determined vertical profiles of oil concentration and ice properties. Including similar measurements of Otsuka et al. (2004), they found that samples with porosity above 0.1 contained oil, and that oil concentration maintained a maximum of approximately 5% by mass for porosities above 0.15. Results did not reveal differences between the 3 different crude oils used, or dependence on warming of the ice prior to excavation. Based on this prior work, we estimate bulk oil entrainment as a constant 4.5% by weight for ice of a porosity above a threshold that we consider to vary between 0.1 and 0.15. Hence, the present study explores the question as to how much oil may be retained in columnar (i.e., congelation) sea ice as a function of the distance of this porosity threshold from the ice–ocean interface. A further motivation for this study derives from the fact that recent work by Wilkinson et al. (2007) has led to improved estimates of oil pooling under sea ice but does not consider the entrainment and immobilization of oil into the high-porosity bottom sea ice layers. A comprehensive model of oil–ice interaction such as those reviewed by Reed et al. (1999), however, requires better estimates and parameterizations of immobilization of oil in the bottom layers. Such processes are also of importance in assessing the impact of oil on sea-ice microbial communities, which are typically concentrated in the very same subvolume of the ice cover.

Methods

To achieve the goals of this study, field measurements of sea ice bulk salinity and temperature profiles were used to calculate porosity profiles under different boundary conditions relevant in the context of oil release under sea ice. These profiles were interpreted in the context of previous work, relating the porosity profile to potential oil entrainment. Salinity data were available for 12 years while temperature profile time series were available for only 6 years. In order to obtain temperature profiles applicable for all cores and to aid in the development of parameterization schemes we

devised three temperature scenarios for each day of the year (cold, average, and warm) and determined three corresponding porosity profiles for each of the salinity cores.

Ice sampling and characterization were carried out in level landfast sea ice in the Chukchi Sea at Barrow, Alaska, between Ukpeagvik Iñupiat Corporation Naval Arctic Research Lab (UIC-NARL) and Point Barrow. The landfast ice at this location is representative of undeformed level ice common in many of the regions targeted for offshore oil and gas development, in particular in the Chukchi and Beaufort Seas. Each year, a location approximately 0.5 to 2 km offshore near Barrow was chosen for repeat measurements. The investigated ice was level first-year ice that started to form between November and December and continued to increase in thickness until the end of May. Water depth was approximately 6 m. In general, a limited amount of snow melt took place in May and meltpond formation began in June (Petrich et al., 2012).

Sea ice cores for salinity determination were taken with a fiberglass core barrel (10 cm diameter) and immediately sectioned into vertical segments on site to minimize loss of brine from the ice (Eicken, 2010). 55 cores used in this study had a vertical sampling size at the bottom of approximately 0.05 m or less and were taken between 2000 and 2011. Of these cores, 8 cores were sampled at a vertical section thickness of 0.03 m or less.

Starting in the winter of 2005/6, an automated probe was used to record profiles of water and ice temperature in vertical intervals of 0.1 m (Druckenmiller et al., 2009). Measurements were performed at intervals of 5 to 30 minutes from January or February until June. In order to determine porosity profiles, the ice temperature profile is needed at the ice–water interface. We determined this profile by determining a best fit curve for adjacent thermistors as described below.

The complete set of salinity and temperature measurements is archived as part of the Seasonal Ice Zone Observing Network (SIZONet) and is available through the Advanced Cooperative Arctic Data and Information Service (ACADIS, http://www.aoncadis.org/; Eicken et al., 2012).

For the ice considered here, the temperature follows an approximately linear profile above the ice–water interface and is depth-independent below the ice–water interface (Petrich and Eicken, 2010). Deviations from the linear profile are most pronounced close to the ice surface where ice temperature responds quickly to air temperature variations and seasonal warming. Since this region is not of interest, the fitting algorithm was restricted to temperature data at least 0.4 m below the ice–snow interface, and no more than 1.0 m above the ice–water interface. For each temperature profile, least-square optimization was used to find the parameters T_w, z_{IF}, dT/dz, and d^2T/dz^2 of the equation

126 $$T(z) = \begin{cases} T_w & \text{for} \quad z - z_{IF} < 0 \\ T_w + \dfrac{dT}{dz}(z - z_{IF}) + \dfrac{d^2T}{dz^2}(z - z_{IF})^2 & \text{for} \quad z - z_{IF} \geq 0 \end{cases}, \qquad (1)$$

127 where T is temperature, z is vertical position, z-z_{IF} is the vertical position above the ice–water
128 interface, T_w is the depth-independent water temperature, dT/dz is the temperature gradient above
129 the ice–water interface (dT/dz<0), and d^2T/dz^2 is the curvature of the ice temperature profile. Visual
130 inspection showed that the second-order fit produces unrealistic results in the presence of strong
131 temperature gradients early in the season. As a result, we performed a linear fit prior to day-of-year
132 65, i.e. d^2T/dz^2=0 was prescribed in Equation (1). The time series of temperature measurements are
133 available through ACADIS.

134 Temperature and salinity were used to calculate profiles of porosity, ϕ, from phase relationships
135 given by Cox and Weeks (1983) and Leppäranta and Manninen (1988) (cf. Petrich and Eicken, 2010).
136 An air content of 0 was assumed since the ice under consideration was below the freeboard line and
137 we are only considering the pore space connected to seawater. Porosity profiles were calculated at 1
138 mm increments based on a linear temperature profile and bulk salinity measured at the
139 corresponding depth.

140 Sea ice data from Barrow, Alaska, were related to oil-in-ice experiments in the Canadian Arctic and
141 laboratory studies, all performed on structurally similar, columnar ice. Laboratory tank experiments
142 were performed under quiescent conditions, and sea ice had a lamellar ice–ocean interface and
143 crystal structure representative of undeformed first-year sea ice at Barrow (Karlsson, 2009; Karlsson
144 et al., 2011). Field experiments were performed under undeformed landfast first-year sea ice in the
145 Canadian Arctic with seawater salinity, water depth, low tidal range (0.3 m), and ice thickness similar
146 to conditions at Barrow (NORCOR, 1975; Druckenmiller et al., 2009; Petrich et al., 2012). The “feeble”
147 under-ice currents in the Canadian Arctic correspond to quiescent conditions in the laboratory
148 (NORCOR, 1975). Bulk sea ice salinity was highest in laboratory experiments and lowest in the
149 Canadian Arctic. However, since oil entrainment is expressed in relation to ice porosity, observations
150 of field and laboratory experiments are comparable (Karlsson et al., 2011).

151 Accessible pore space was defined as the volume below the lowest horizon of threshold porosity ϕ,
152 z_x. This threshold porosity was motivated by bounds on oil entrainment summarized by Karlsson et
153 al. (2011). Oil entrainment was observed in ice of ϕ>0.10, with saturated entrainment beginning at
154 ϕ>0.15. Hence, entrainment depth z_x was calculated for both ϕ=0.10 and ϕ=0.15 in order to estimate
155 the range of likely entrainment volumes.

Because bulk salinity and porosity change appreciably over a narrow range at the ice–ocean interface (Notz and Worster, 2008), penetration depths were included in the quantitative analysis only if they exceeded the thickness of the bottom-most salinity samples. However, excluded depths are plotted for completeness.

In oil-entrained sea ice samples, crude oil has been found to occupy typically 4.5%-mass by mass of sea ice. For a typical oil density around 800 kg/m^3 this translates into entrainment of 5.5% by volume. The volume of entrained oil was therefore calculated as 5.5% of the entrainment depth z_x.

Results

Sea ice salinity cores extracted from the ice between 2000 and 2011 show consistency of ice thickness as evident in Figure 1 which plots the length of all cores as a function of day of year. Ice thickness increased from approximately 0.6 m in January to 1.5 m in May. The inter-annual variability in ice thickness was approximately ±0.15 m for any given day of year. The consistency in ice thickness enables analysis without taking ice thickness into account explicitly. At the same time, the observed evolution of ice thickness is representative both of landfast ice and of undeformed level first-year ice that formed during fall freeze-up in the open ocean of the Chukchi and Beaufort Seas.

Temperature gradients at the ice–ocean interface were calculated from the vertical temperature profiles for 2006 to 2011. Figure 2 shows that the temperature gradient at the interface tended to decrease over the course of the season, which is expected due to a combination of increasing ice thickness, snow depth, and air temperatures. Three temperature scenarios at the ice–water interface were derived from these data, representing cold, average, and warm ice conditions. The cold and warm scenarios correspond to the most extreme observations in the data record, while the average scenario represents the typical development of the temperature gradient. Temperature profiles of the respective scenarios were defined using

$$T(z) = T_w + \frac{dT}{dz}(z - z_{IF}), \tag{3}$$

with water temperature T_w=-1.8 °C. The scenario-dependent temperature gradient was defined as

$$\frac{dT}{dz} = \left(\frac{dT}{dz}\right)_{DOY=15} + \left[\left(\frac{dT}{dz}\right)_{DOY=150} - \left(\frac{dT}{dz}\right)_{DOY=15}\right]\frac{DOY-15}{135}, \tag{4}$$

where *DOY* is the day of year and temperature gradients on *DOY*=15 and 150 are listed in Table 1.

183 Porosity profiles were calculated based on the measured salinity profiles and representative
184 temperature profiles of Equation (3). A typical example profile is shown in Figure 3. The expected
185 depth of penetration z_x, i.e. the distance of the porosity threshold from the ice–water interface, is
186 shown in Figures 4 and 5 for ϕ=0.10 and 0.15, respectively. Data are scattered but a trend is
187 discernible that shows that the penetration depth increases from January to May in all cases. Also,
188 penetration depth increases with ice temperature. Key data derived from a linear best fit are given in
189 Table 1. For the average temperature scenario, depth to ϕ=0.10 increases from 0.04 m in mid
190 January to 0.12 and 0.18 m at the end of March and May, respectively (Figure 4b). For ϕ=0.15, no
191 numbers were derived for mid January because the depth is less than the thickness of the bottom-
192 most samples in all cases. However at the end of March and May depths are half of the respective
193 values determined for ϕ=0.10 (Figure 5b). Depending on the temperature scenario, derived depths of
194 fluid penetration range from 0.02 to 0.10 m in January to 0.12 to 0.25 m in May for a porosity
195 threshold of 0.10 (Figures 4a and c).

196 The potential oil entrainment based on both ϕ =0.1 and 0.15 is given in Table 1. Entrainment
197 volumes increase with the season and are higher during a warm spell than during a cold spell. While
198 entrainment during a cold spell in January is expected to be less than 1 L/m^2, entrainment could be
199 as high as 5 to 10 L/m^2 during a warm spell in late March. By the end of May, entrainment of 4 to
200 13 L/m^2 should be expected, depending on ice temperature.

201 Discussion

202 Calculated depths of entrainment shown in Figures 4 and 5 scatter. This may be due to at least two
203 factors: the way porosity was calculated and the stochastic nature of the spatial bulk salinity
204 distribution. Scatter is expected due to the way porosity was calculated. While the temperature
205 profile used is a continuous function with depth, the bulk salinity profile is discontinuous at the edges
206 of the sample volumes. The resulting porosity profile reflects this step profile, introducing a vertical
207 uncertainty of plus or minus one half of the vertical sample size (i.e., ±0.025 m in most cases).
208 However, this effect cannot explain the range of scatter observed toward May.

209 Scatter is also to be expected on physical grounds as each data point is derived from a single salinity
210 core and salinity core data are known to contain a stochastic component (e.g. Bennington, 1967;
211 Gough et al., 2012). For example, Gough et al. (2012) found that salinity between cores must differ
212 by at least 29% for them to be considered different with 90% confidence. This can be converted into
213 an estimate of the expected scatter in depth z_x for Figure 4b (i.e., z_x based on ϕ=0.10 for average ice

temperatures) from the relationship between bulk salinity, porosity and temperature: in linear approximation, the phase relationship takes on the form

$$\phi \propto \frac{S}{T_w + \frac{dT}{dz}(z - z_{IF})}, \quad (5)$$

where S is the bulk sea ice salinity. For any particular porosity ϕ, an uncertainty in S of ±14.5% (i.e., the window of 29% given by Gough et al. (2012)) is equivalent to a temperature range of ±14.5%. At a temperature of -2.5 °C (e.g., ϕ=0.10 if S=5), this temperature range of ±0.36 °C corresponds to an uncertainty of the vertical position z of ±0.024 and ±0.18 m for dT/dz=-15 and -2 °C/m, respectively. Hence, scatter expected around the best fit line in Figure 4b is ±0.024 m and ±0.18 m in mid January and late May, respectively. The range spanned by data in Figure 4b is actually smaller than this (±0.02 and ±0.10 m, respectively), supporting the conclusion that the scatter observed is consistent with expectations due to natural variability of sea ice bulk salinity.

Brine loss from the bottom-most layers of sea ice may impact measured salinities and hence derived porosities. As shown by Notz and Worster (2008), in thin young ice, as much as the bottom 5 cm may greatly exceed porosities of 0.1 to 0.2, with near-constant lower porosities above this bottom layer. For thicker ice (>0.1m) the high porosity of the bottom-most few cm appears to result in a substantial underestimation of the bulk salinity and hence brine volume fraction, even for rapid on site sampling as practiced here. While the determination of the location of the 0.1 or 0.15 porosity horizons for thicker ice is less impacted by such brine loss, brine loss during sampling would result in a slight underestimate of entrainment depth and hence underestimate of oil entrainment. At the same time, since simultaneous measurements of ice salinity and oil content in high porosity regions (ϕ>0.3) are not available, the initial assumption of porosity-independence of oil content could be violated. In this case, the volume fraction of oil entrained into sea ice will likely be underestimated. For example, if we assume as an upper limit an oil volume fraction of 30% in the bottom-most 3 to 10 mm of sea ice, this effect might increase the amount of oil entrained per square meter by up to 1-3 liters.

A distinction should be emphasized between the influence of warm and cold spells and years with systematically above- or below-normal ice temperatures. Bulk salinity depends on the temperature profile at the time of ice formation in a way that higher temperatures generally lead to the formation of less saline ice (e.g. Kovacs, 1996; Petrich et al., 2006, 2011). Hence, while brief warm periods increase porosity temporarily (Equation 5), extended warm periods decrease interface porosity by resulting in the formation of low-salinity ice. This is illustrated by data of 2010, which experienced comparatively high ice temperatures (Figure 2), resulting in slower growth rates and lower bulk

245 salinity (not shown). The lower bulk salinity is reflected in Figures 4 and 5 as smaller entrainment
246 depths from March onward, in spite of generally warm ice temperatures. The net effect of this
247 feedback is that entrainment depth z_x may be unseasonally large in ice warming up after having
248 grown under colder-than-average conditions. Anomalies in the snow cover at the site of interest can
249 have a comparable impact, such that deeper-than-normal snow cover will tend to decrease ice
250 growth rates and hence salinities over the course of the season. For ice types with substantially
251 different roughness, such as ridged or rubbled ice, locally variable snow depth may result in spatially
252 variable oil entrainment potential.

253 Entrainment of oil in the interstitial space of the ice matrix can be expected to contribute to the oil
254 pooling capacity of warm ice. Two methods have been used to estimate the expected pooling of oil in
255 under-ice depressions (Wilkinson et al., 2007). Traditionally, only statistical information on ice
256 topography has been used to assess pooling potential. Following the statistical method, oil pooling is
257 assumed to take place in all pronounced depressions, and capacity has been estimated to average at
258 30 L/m^2 (Wilkinson et al., 2007). However, more recent calculations based on actual under-ice
259 topography and a gravity flow model suggested that pooling may only result in retention of 4 L/m^2
260 (Wilkinson et al., 2007). In the gravity flow model, oil is distributed assuming the absence of currents
261 (consistent with field and laboratory experiments used in this study), while the oil distribution
262 mechanism is undefined in the statistical model. Oil entrainment in the interstitial space of the ice
263 matrix adds to the pooling capacity. For the case of landfast ice at Barrow, Alaska, it was found that
264 entrainment volumes of 10 L/m^2 may be observed in warm ice. These entrainment volumes are valid
265 for ice that is homogeneously oil-covered over a hitherto unspecified period required for
266 entrainment (the time scale is likely to be of the order of hours or days (NORCOR, 1975)). Based on
267 the two different methods mentioned above, 50% and 9% of the ice underside is expected to be oil-
268 covered, respectively (Wilkinson et al., 2007). Hence, the effective entrainment averaged over a large
269 scale would also be reduced to 50% or 9% of the values given in Table 1, respectively. Based on
270 10 L/m^2 entrainment in warm ice, an areal coverage of 50% and 9% for the statistical estimate and
271 the gravity model, would contribute an additional 15% and 25%, respectively, to the oil retention
272 capacity under ice.

273 Conclusion

274 Based on a 12-year record of salinity data and 6 years of ice temperature data at Barrow, Alaska, we
275 find that the potential volume of oil entrained in the interstitial space of the sea ice crystal fabric
276 increases from January to May. Entrainment may reach approximately 20% of the potential oil
277 volume pooled beneath sea ice, with the latter based on estimates by Wilkinson et al. (2007).

Analyses for different regions could be performed based on available sea ice salinity and ice temperature data. Further, entrainment depths determined in this study would be relevant beyond the scope of oil entrainment, for example in the context of habitat available for ice biota.

In the context of oil-spill impact assessment it will be valuable to assess the mechanism and rate of oil entrainment as there is no evidence that oil, once entrained in the ice continues to spread laterally (NORCOR, 1975; Martin, 1979). Further, two mechanisms related to the presented work could lead to a drastic increase of the entrainment potential. These are vertical migration of oil through the ice leading to release at the surface at the end of May (NORCOR, 1975; Karlsson et al., 2011), and the formation of Arctic platelet ice due to meltwater beneath sea ice (Jeffries et al., 1995). As shown by Eicken (1994), such ice formation is particularly prominent in bottom ice surface depressions and hence likely to trap and potentially greatly increase the entrainment potential for oil. A quantitative assessment and modeling of these processes would improve and could potentially alter response to oil spills. The results of this study indicate that oil entrainment in the interstitial space between ice crystals contributes to oil spatial fixation and temporary removal from the oceans.

Acknowledgements

This work was funded by The Norwegian Research Council, project number 195160, and Eni Norge. Data at Barrow, Alaska, were acquired under research grants OPP-0632398 and OPP-0856867, with additional support from grant OPP-0934683, of the National Science Foundation, USA. The constructive comments of two anonymous reviewers are gratefully acknowledged.

References

Bennington, K. O. (1967), Desalination features in natural sea ice, J. Glaciol., 6(48), 845–857.

Buist, I., R. Belore, D. Dickins, D. Hackenberg, A. Guarino, and Z. Wang (2008), Empirical Weathering Properties of Oil in Ice and Snow. Final Report. Project Number 1435-01-04-RP-34501, U.S. Department of the Interior Minerals Management Service, Anchorage, Alaska, USA. 170 pp.

Cota, G. F., and R. E. H. Smith (1991), Ecology of bottom ice algae: II. Dynamics, distributions and productivity, J. Mar. Systems ,2, 279–295.

Cox, G. F. N., and W. F. Weeks (1975), Brine drainage and initial salt entrapment in sodium chloride ice, Research Report 345, Cold Regions Research and Engineering Lab, Hanover, NH, USA, 88 pp.

Cox, G. F. N., and W. F. Weeks (1983), Equations for determining the gas and brine volumes in sea-ice samples. J. Glaciol., 29(102), 306–316.

Dickins, D. F. (1992), Behavior of Spilled Oil at Sea (BOSS): Oil-in-Ice Fate and Behavior, Environment Canada, U.S. Minerals Management Service, and American Petroleum Institute. 342 pp.

Dickins, D. F. (2011), Behavior of Oil Spills in Ice and Implications for Arctic Spill Response. In: Proceedings of the OTC Arctic Technology Conference, 7-9 February 2011, Houston, Texas, USA, OTC 22126, 1–15.

Druckenmiller, M. L., H. Eicken, M. A. Johnson, D. J. Pringle and C. C. Williams (2009), Toward an integrated coastal sea-ice observatory: System components and a case study at Barrow, Alaska. Cold Regions Science and Technology, 56, 61–72.

Eicken, H., R. Gradinger, M. Kaufman and C. Petrich. (2012), Sea-ice core measurements (SIZONET). Dataset 26 August 2008, updated 2012. UCAR/NCAR – CISL – ACADIS. doi:10.5065/D63X84KG

Eicken, H. (2010), Ice sampling and basic sea ice core analysis. In Field Techniques for Sea Ice Research, Eicken, H. et al. (eds), University of Alaska Press, 117–140.

Eicken, H. (1994), Structure of under-ice melt ponds in the central Arctic and their effect on the sea-ice cover. Limnol. Oceanogr., 39(3), 682-694.

Eide, L., and S. Martin (1975), The formation of brine drainage features in young sea ice, J. Glaciol., 14, 137–154.

Fingas, M. F., and B. P. Hollebone (2003), Review of behavior of oil in freezing environments. Mar. Pollut. Bull., 47, 333–340.

Gradinger, R. R., M. R. Kaufman, B. A. Bluhm (2009), Pivotal role of sea ice sediments in the seasonal development of near-shore Arctic fast ice biota, Mar. Ecol. Prog. Ser., 394, 49–63.

Gough, A. J., A. R. Mahoney, P. J. Langhorne, M. J. M. Williams, and T. G. Haskell (2012), Sea ice salinity and structure: A winter time series of salinity and its distribution, J. Geophys. Res., 117, C03008, doi:10.1029/2011JC007527.

Jeffries, M. O., K. Schwartz, K. Morris, A. D. Veazey, H. R. Krouse, and S. Gushing (1995), Evidence for platelet ice accretion in Arctic sea ice development, J. Geophys. Res., 100(C6), 10,905–10,914, doi:10.1029/95JC00804.

Karlsson, J. (2009), Oil movement in sea ice. Masters Thesis, University of Copenhagen, Copenhagen, Denmark, 199 pp.

Karlsson, J., C. Petrich, and H. Eicken (2011), Oil entrainment and migration in laboratory-grown saltwater ice. Proceedings of the 21st International Conference on Port and Ocean Engineering under Arctic Conditions 10-14 July 2011, Montréal, Canada. POAC11-186, 1–10.

Krembs, C., R. Gradinger, M. Spindler (2000), Implications of brine channel geometry and surface area for the interaction of sympagic organisms in Arctic sea ice, Journal of Experimental Marine Biology and Ecology, 243, 55–80.

Kovacs, A. (1996), Sea ice: Part I. Bulk salinity versus ice floe thickness. Report 96-7, Cold Regions Research and Engineering Laboratory, Hanover, NH, USA. 23pp.

Leppäranta, M., and T. Manninen (1988), The brine and gas content of sea ice with attention to low salinities and high temperatures. Finnish Institute of Marine Research Internal Report 1988(2). 15 pp.

Martin, S. (1979), A field study of brine drainage and oil entrainment in first-year sea ice. J. Glaciol. 22, 473–502.

NORCOR (1975), The Interaction of Crude Oil with Arctic Sea Ice, Beaufort Sea Technical Report 27, Department of the Environment, Canada, 213pp.

Notz, D., and M. G. Worster (2008), In situ measurements of the evolution of young sea ice. J. Geophys. Res., 113, C03001, 1–7, doi:10.1029/2007JC004333.

353 Otsuka, N., H. Kondo, H. Saeki (2004), Experimental study on the characteristics of oil ice
354 sandwich. Proceedings of OCEANS '04 MTS/IEEE—TECHNO-OCEAN '04., vol. 3, 9–12 Nov. 2004,
355 Kobe, Japan. pp. 1470–1475.

356 Petrich, C., and H. Eicken (2010), Growth, structure, and properties of sea ice. In Sea Ice, 2nd ed.,
357 Thomas, D. N., and G. S. Dieckmann (eds), Wiley-Blackwell, 23–77.

358 Petrich, C., P. Langhorne, and H. Eicken (2011), Modelled bulk salinity of growing first-year sea ice
359 and implications for ice properties in spring. Proceedings of the 21st International Conference on
360 Port and Ocean Engineering under Arctic Conditions 10-14 July 2011, Montréal, Canada. POAC11-
361 187, 1–10.

362 Petrich, C., H. Eicken, J. Zhang, and J. R. Krieger, Y. Fukamachi, and K. I. Ohshima (2012), Coastal sea
363 ice melt and break-up in northern Alaska: processes and possibility to forecast, J. Geophys. Res., 117,
364 C02003, 1–19, doi: 10.1029/2011JC007339.

365 Reed, M., O. Johansen, P. J. Brandvik, P. Daling, A. Lewis, R. Fiocco, D. Mackay, R. Prentki (1999), Oil
366 spill modeling towards the close of the 20th century: Overview of the state of the art. Spill Sci.
367 Technol. Bull., 5(1), 3-16.

368 Weissenberger, J., G. Dieckmann, R. Gradinger, and M. Spindler (1992), Sea ice: A cast technique to
369 examine and analyze brine pockets and channel structure, Limnol. Oceanogr., 37(1), 179-183.

370 Wilkinson, J. P., P. Wadhams, and N. E. Hughes (2007), Modelling the spread of oil under fast sea ice
371 using three-dimensional multibeam sonar data, Geophys. Res. Lett., 34, L22506,
372 doi:10.1029/2007GL031754.

373 Wolfe, L. S., and D. P. Hoult (1974), Effects of oil under sea ice. J. Glaciol., 13(69), 473–488.

374

Tables

Table 1. Temperature gradients dT/dz (Figure 2), entrainment depths z_x, and oil content at day-of-year 15, 90, and 150, representing beginning, middle, and end of the data record, respectively. Entrainment depths are given for porosity thresholds 0.1 (Figure 4) and 0.15 (Figure 5). Oil content is calculated from entrainment depths assuming 5.5% entrainment by volume and ϕ=0.15, (values for ϕ=0.1 given in brackets)

Scenario	**Cold**			**Average**			**Warm**		
Day of Year	15	90	150	15	90	150	15	90	150
dT/dz (°C/m)	-30	-16	-4	-15	-8	-2	-7.5	-4	-1
z_x (m), ϕ=0.10	0.02	0.08	0.12	0.04	0.12	0.18	0.10	0.18	0.25
z_x (m), ϕ=0.15		0.04	0.07		0.06	0.09		0.08	0.10
Oil (L/m^2)	(1)	2 (4)	4 (7)	(2)	3 (7)	5 (10)	(5)	4 (10)	5 (13)

Figure Captions

Figure 1. Ice thickness, *H*, of salinity cores used in this study as a function of Day-of-Year (*doy*). The dashed line follows the best fit line $H = 0.59\ \text{m} + 0.013\ \text{m}\ doy - 4.4\text{x}10^{-5}\ \text{m}\ doy^2$, the dotted lines delineate the ±0.15 m interval around the dashed line.

Figure 2. Ice temperature gradients at the ice–ocean interface, dT/dz, derived from temperature probe data as a function of day-of-year. The dashed line indicates the average temperature scenario used, while the upper and lower thin solid lines indicate warm and cold scenarios, respectively.

Figure 3. Example of (a) temperature, (b) salinity and (c) porosity profiles under the average temperature scenario applied to salinity data of 29 April 2008. Temperature and porosity were calculated for the bottom-most 0.4 m. The dashed lines in (c) mark the depths of porosity 0.10 and 0.15, respectively.

Figure 4. Oil penetration depth based on porosity threshold ϕ=0.1 for temperature scenarios (a) warm, (b) average, and (c) cold. The length of vertical lines indicates penetration depths within the bottom-most salinity sample that were excluded from the quantitative analysis. The dashed best fit lines indicate the general trend of the respective scenarios.

Figure 5. Oil penetration depth based on porosity threshold ϕ=0.15 for temperature scenarios (a) warm, (b) average, and (c) cold. The length of vertical lines indicate penetration depths within the bottom-most salinity sample that were excluded from the quantitative analysis. The dashed best fit lines indicate the general trend of the respective scenarios.

Figures

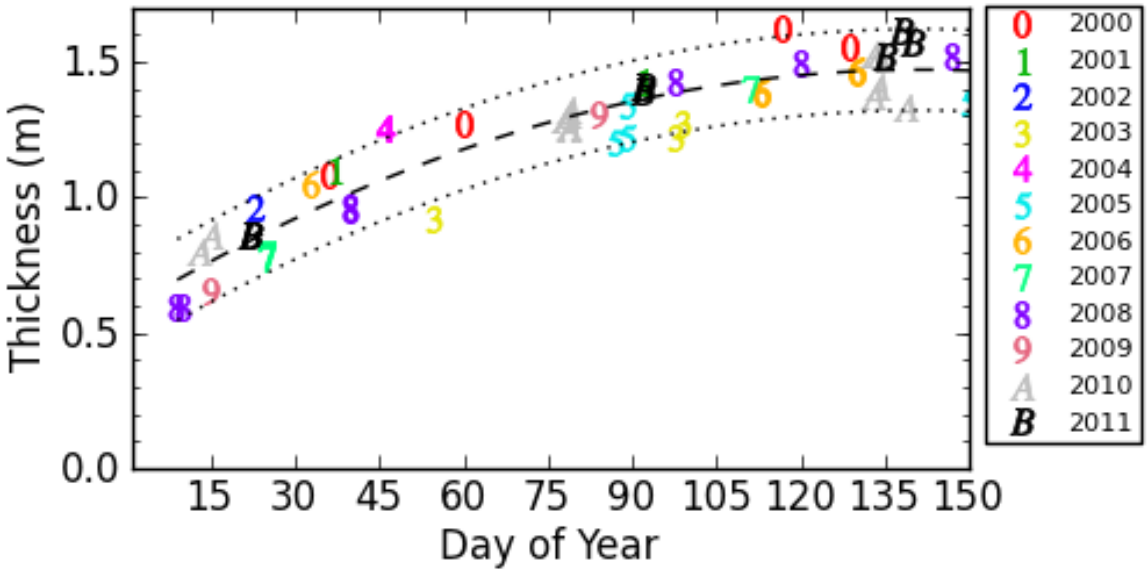

Figure 1. Ice thickness, *H*, of salinity cores used in this study as a function of Day-of-Year (*doy*). The dashed line follows the best fit line H =0.59 m+0.013 m doy – 4.4x10^{-5} m doy^2, the dotted lines delineate the ±0.15 m interval around the dashed line.

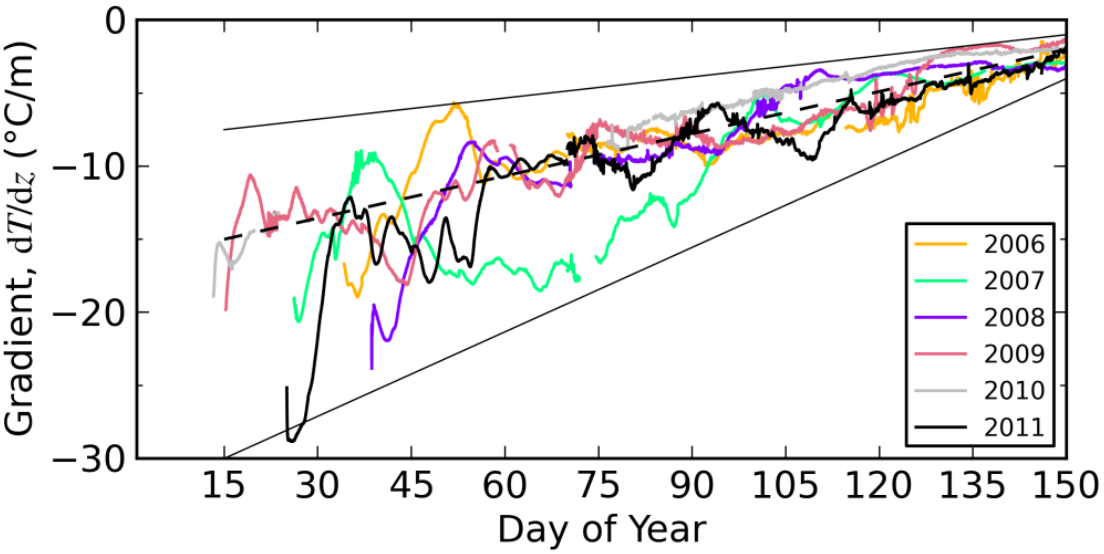

Figure 2. Ice temperature gradients at the ice–ocean interface, d*T*/d*z*, derived from temperature probe data as a function of day-of-year. The dashed line indicates the average temperature scenario used, while the upper and lower thin solid lines indicate warm and cold scenarios, respectively.

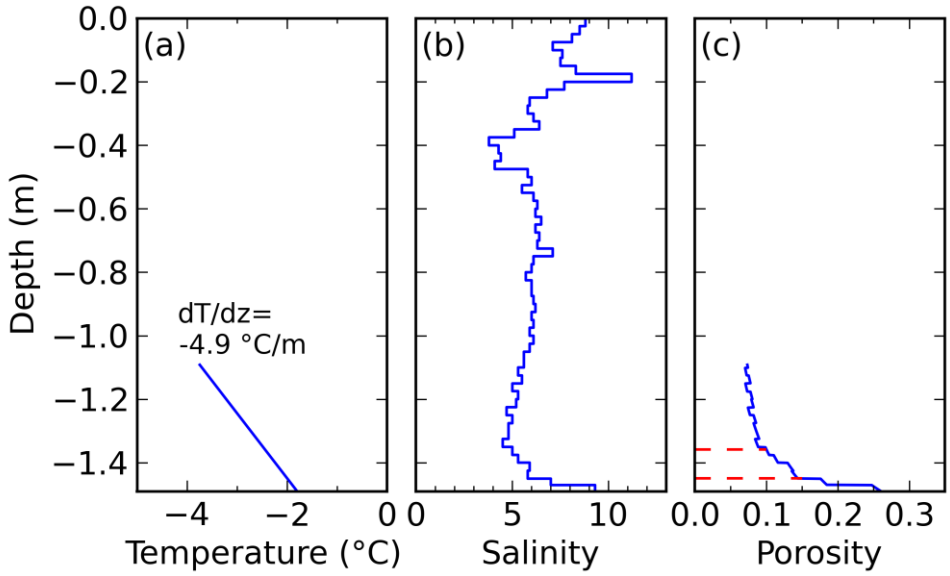

418

419 Figure 3. Example of (a) temperature, (b) salinity and (c) porosity profiles under the average
420 temperature scenario applied to salinity data of 29 April 2008. Temperature and porosity were
421 calculated for the bottom-most 0.4 m. The dashed lines in (c) mark the depths of porosity 0.10 and
422 0.15, respectively.

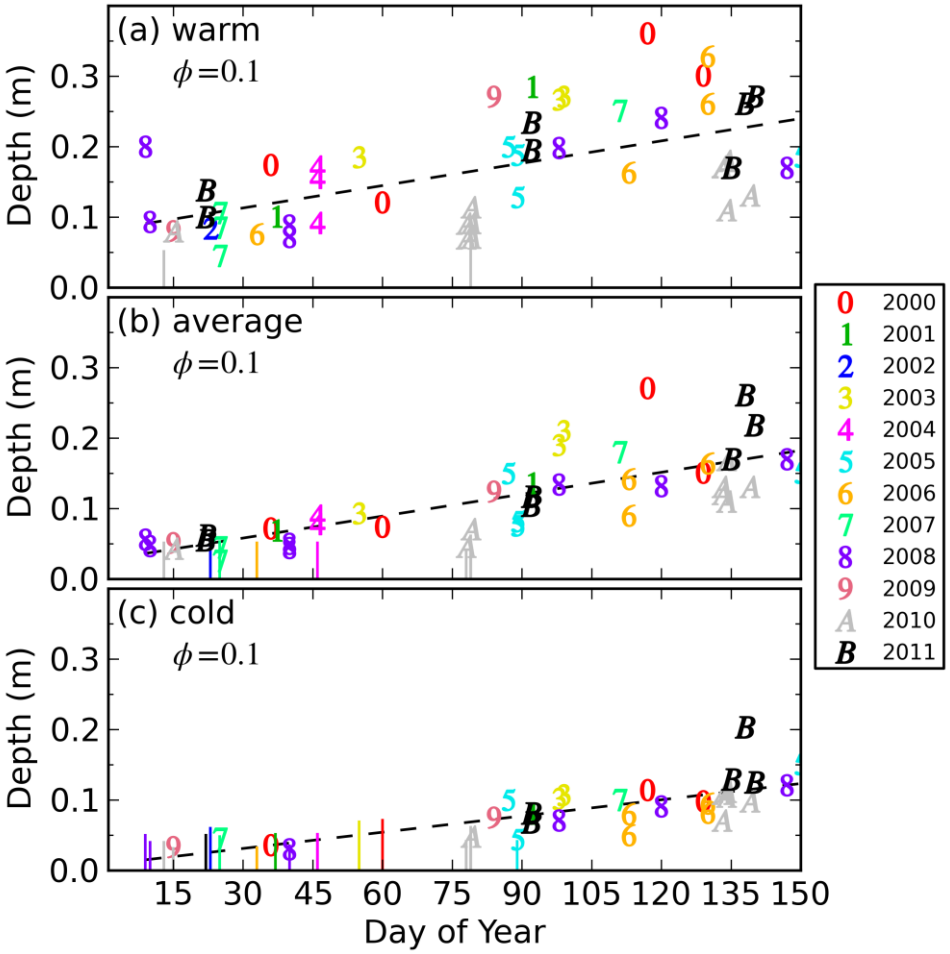

Figure 4. Oil penetration depth based on porosity threshold ϕ=0.1 for temperature scenarios (a) warm, (b) average, and (c) cold. The length of vertical lines indicates penetration depths within the bottom-most salinity sample that were excluded from the quantitative analysis. The dashed best fit lines indicate the general trend of the respective scenarios.

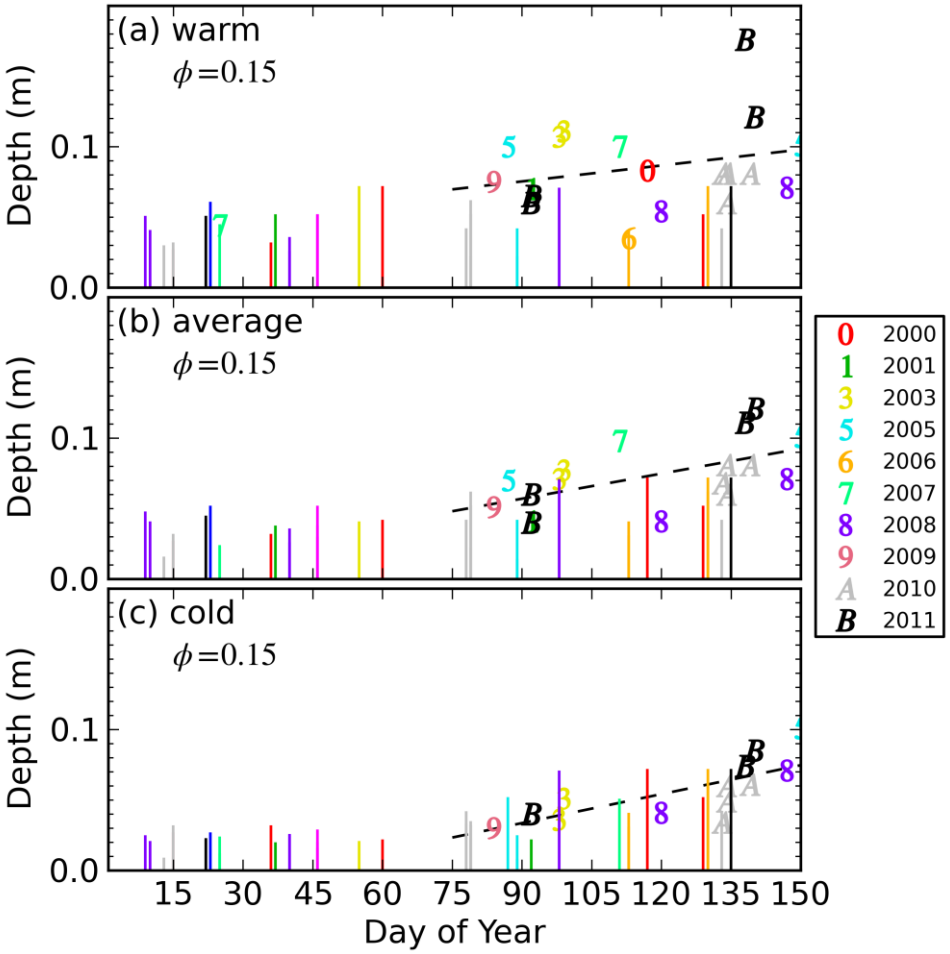

Figure 5. Oil penetration depth based on porosity threshold ϕ=0.15 for temperature scenarios (a) warm, (b) average, and (c) cold. The length of vertical lines indicate penetration depths within the bottom-most salinity sample that were excluded from the quantitative analysis. The dashed best fit lines indicate the general trend of the respective scenarios.